Geothermics 64 (2016) 135–151

Contents lists available at ScienceDirect

Geothermics

journal homepage: www.elsevier.com/locate/geothermics

Numerical modelling of thermal convection in the Luttelgeest carbonate platform, the Netherlands

Lindsay Lipsey[a,b,*], Maarten Pluymaekers[b], Tatiana Goldberg[b], Katrien van Oversteeg[a,b], Lilya Ghazaryan[b], Sierd Cloetingh[a], Jan-Diederik van Wees[a,b]

[a] Faculty of Geosciences, Utrecht University, PO Box 80.021, 3508 TA Utrecht, The Netherlands
[b] TNO, PO Box 80015, 3508 TA Utrecht, The Netherlands

ARTICLE INFO

Article history:
Received 16 December 2015
Received in revised form 9 May 2016
Accepted 11 May 2016
Available online 25 May 2016

Keywords:
Geothermal energy
Thermal convection
3D numerical modelling
Temperature anomaly
Fracture permeability

ABSTRACT

The presence of convective fluid flow in permeable layers can create zones of anomalously high temperature which can be exploited for geothermal energy. Temperature measurements from the Luttelgeest-01 (LTG-01) well in the northern onshore region of the Netherlands indicate variations in the thermal regime that could be indicative of convection. This thermal anomaly coincides with a 800 m interval of Dinantian carbonates showing signs of increased fracture permeability of 6 10^{-14} m^2.

In this study, we reproduce the thermal gradient at LTG-01 using 3D numerical models in order to better understand the interplay between natural fracture permeability and temperature patterns. Numerical models of thermal convection are used to illustrate the role of permeability on the timing of convection onset, convection structure development and resulting temperature patterns.

Rayleigh number calculations indicate that convective flow is realistic within the Luttelgeest carbonate platform. The degree and pattern of convection depends strongly on the platform geometry and thickness, permeability structure and geothermal gradient of the convective zone. The spacing of convective upwellings and their thermal anomalies can be well predicted by numerical models that provide evidence for significant convection-driven thermal anomalies. Numerical models can facilitate in exploration workflows to assess thermal variation and location of upwelling zones.

1. Introduction

Thermal anomalies in deep sedimentary layers and basement rock are largely controlled by convective fluid flow within permeable zones. Convection is of particular interest in geothermal energy, as the up flow of hot fluids yields relatively shallow high-temperature anomalies, which are preferential targets for geothermal exploration. In fact, numerical studies show that convective fluid flow leaves a distinct pattern on the local geothermal gradient. The thermal effect is critically dependent on the pre-existing thermal gradient, thickness and permeability (e.g. Pasquale et al., 2013).

Owing to oil and gas exploration, the accessibility of subsurface temperature data has assisted in our understanding of temperature patterns. Analyses have revealed significant thermal anomalies located in graben systems and sedimentary basins, several of which were interpreted to be the result of thermal convection (Garibaldi et al., 2010; Bonté et al., 2012; Pasquale et al., 2013; Guillou-Frottier et al., 2013). These studies have used a combination of numerical tools to link deep temperatures, geological structures and fluid flow. Guillou-Frottier et al. (2013) use 2D numerical models to reproduce thermal features observed in the Upper Rhine Graben in fractured granitic basement and thick sedimentary layers at shallow depth. The models help to understand how convective cells establish and show that these anomalously hot zones can only be explained by fluid circulation (Baillieux et al., 2013). At larger depth, Pasquale et al. (2013) argue that a thick carbonate unit in the Po Plain may host thermal convection, which would explain the lower geothermal gradient within the carbonate layer and the higher gradient in the overlying layers. This particular thermal signature is thought to be characteristic of convection processes. They quantified the potential for thermal convection by performing Rayleigh number analyses and calculate the minimum thermal gradient that is required for convection based on permeability and thickness.

While both reservoir and basin scale modelling have been used to address thermal features characteristic of convective fluid flow, to date there have been no 3D numerical modelling studies which

* Corresponding author at: Faculty of Geosciences, Utrecht University, PO Box 80.021, 3508 TA Utrecht, The Netherlands.
E-mail address: l.c.lipsey@uu.nl (L. Lipsey).

http://dx.doi.org/10.1016/j.geothermics.2016.05.002

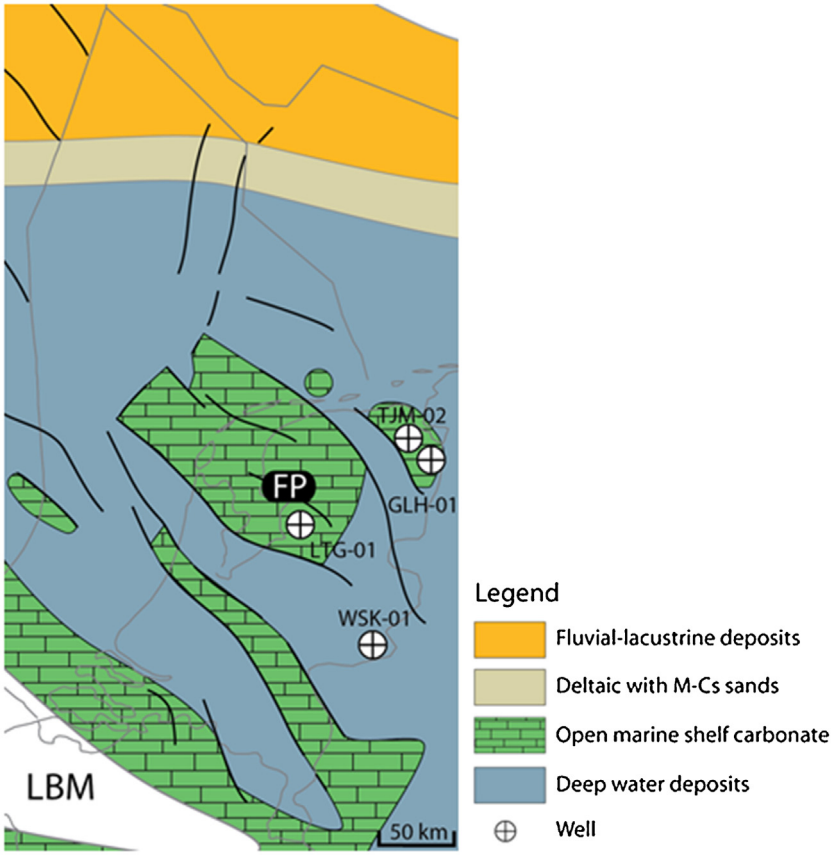

Fig. 1. Paleogeographic map of the Netherlands during the Early Carboniferous. LBM: London-Brabant Massif; FP: Friesland Platform. (Adapted after Kombrink, 2008).

focus on deep carbonate reservoirs in detail. In the Netherlands, renewed interest in deeper formations has led to the drilling of several deep wells. Recent work on the temperature distribution in the Dutch subsurface revealed a thermal anomaly at 4–5 km depth at one of the deep wells, Luttelgeest-01 (LTG-01), which could be explained by thermal convection. Temperature measurements show a shift to higher temperatures at depths greater than 4000 m, corresponding to the Dinantian carbonate interval. The local thermal gradient strongly resembles the thermal signature that is believed to be characteristic of convective processes.

The aim of the study is to reproduce the temperature pattern at Luttelgeest through 3D numerical models of thermal convection in order to elucidate possible flow and thermal structures. This is done to better understand the interplay between geothermal anomalies, platform geometry and natural permeability. Numerical experiments are used to test the effect of platform geometry and the permeability structure on the development of thermal convection and resulting temperature patterns.

First we introduce the geological setting of the Luttelgeest platform, and subsequently present the evidence for convection from temperature data, permeability measurements on cores and determine the minimum permeability required for convection using the Rayleigh number analysis. Determining whether convection is possible is important for predicting and understanding the likely distribution of geothermal resources in deep carbonate layers. Following this, we use site-specific fluid and rock properties to perform numerical simulations of thermal convection. Results from numerical simulations are used to illustrate the type of behaviour that may occur, in terms of flow paths and temperature patterns. The numerical simulations allow for a better understanding of the nature and evolution of convective flow.

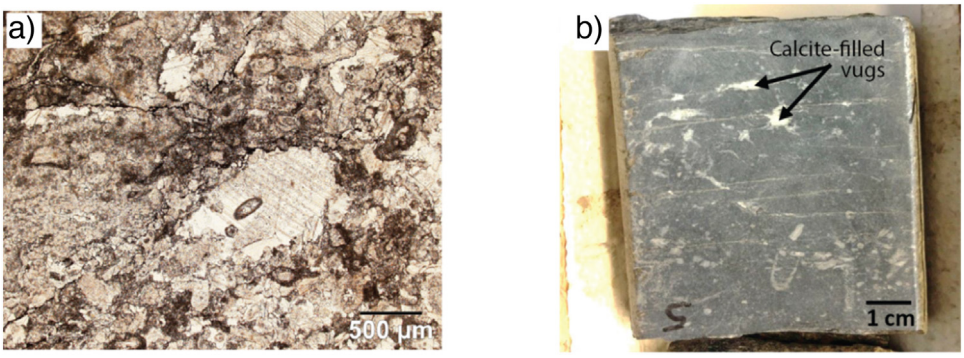

Fig. 2. (a) Thin section from a sample at depth 4376 m. Bioclastic packstone. Note abraded and fragmented crinoid plate in the center and sutured stylolites with insoluble residue in black. Plane poloarized light. (b) Sample from the core of Dinantian carbonate interval (depth 4376 m). Note the vugs filled with sparitic calcite.

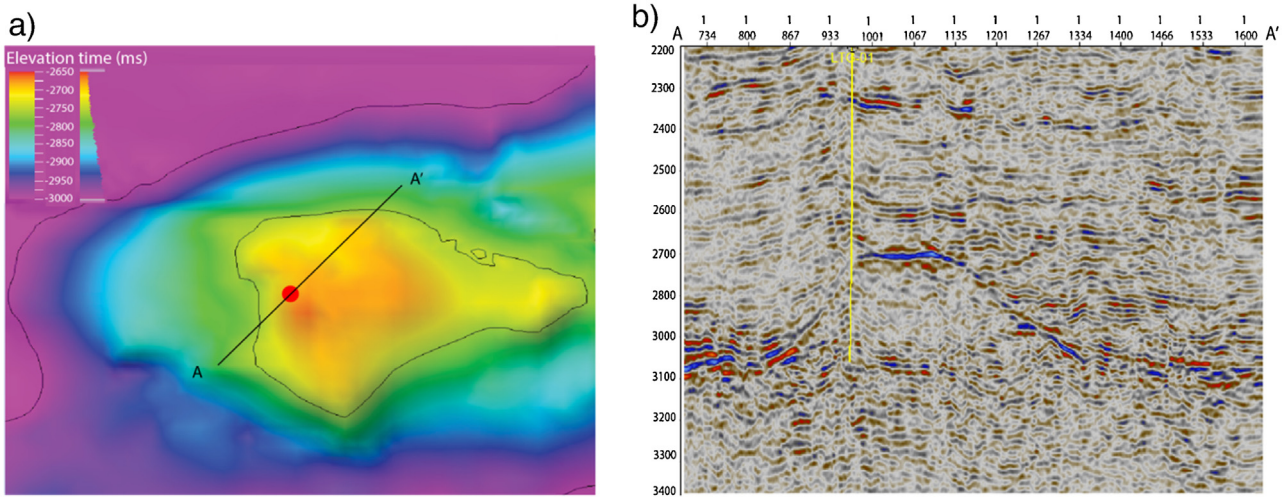

Fig. 3. (a) Top view of the Luttelgeest platform. The LTG-01 well is indicated in red. (b) Seismic section A–A'. The LTG-01 well is indicated in yellow. Note the location of the well along the margin of the platform.

2. Geology

2.1. Geological setting

In Carboniferous times the Netherlands and surrounding areas were part of a large intra-cratonic basin known as the Northwest European Carboniferous Basin (NWECB) (Kombrink et al., 2010). The basin is delineated by the Mid north Sea High to the north and the London-Brabant Massif to the south. It formed in response to renewed back-arc extension in the Rhenohercynian basin, which occurred following the Caledonian orogeny during mid-Devonian times. This initiated the formation of a series of linked NW-SE trending fault blocks. During the Dinantian the Netherlands part of the NWECB experienced a tensional regime, resulting in a horst-and-graben complex (Kombrink et al., 2010) (Kombrink, 2008) (Fig. 1).

Differential subsidence of this horst-and-graben topography strongly influenced sedimentation and facies distribution during the Carboniferous (Kombrink et al., 2010). While fluvial systems dominated the Mid North Sea High, horst blocks effectively shielded large regions further south from siliclastic influx (Van Hulten, 2012). This created an ideal environment for widespread carbonate platform development on hanging-wall blocks during the Dinantian. Late Visean sea level lowering left platforms locally subaerially exposed, inducing significant leaching and karstification. Ultimately, Namurian sea-level transgression caused the platforms to become gradually flooded (Geluk et al., 2007).

The present day stress regime in the Netherlands is extensional with maximum horizontal stress oriented NW-SE (De Jager, 2007). Many structural elements show a characteristic rhomboid pattern of intersecting fault trends. The dominant family of faults trend NW-SE and formed during the mid-Devonian and Early Carboniferous. The trend was reactivated during the Early Permian in response to Late-Variscan wrench faulting and thermal uplift. A conjugate set of NNE-SSW faults developed regionally (De Jager, 2007). Rift basins and platforms appear to share a similar fault pattern, despite having significant differences in structural development (Van Hulten, 2012). The high degree of fault parallelism suggests that faults were repeatedly reactivated under different stress regimes throughout the Netherlands geologic history (Kombrink et al., 2010).

Dinantian carbonates in the Dutch subsurface have varying geometries and show a large range of reservoir quality. These variances reflect differences in tectonic setting, sea level and burial/diagenesis history between areas. A high variability in carbonate sedimentology means that the mechanical properties of carbonate platforms are expected to be heterogeneous and affect the characteristics of fractures. Diagenesis results from a series of processes that develop in response to the availability of fluids and reactants within a given tectonostratigraphic framework. The resultant porosity/permeability architecture develops in response to these depositional events (Goldscheider et al., 2010).

The framework of the Dinantian carbonates in the central part of the NWECB is poorly constrained. With the Upper Carboniferous generally regarded as the lower limit of the economic fairway, there is a scarcity of wells that penetrate the base of the Carboniferous (Van Hulten, 2012). The wells that do are clustered along the NWECB margins. Seismic reflections are often hard to distinguish, making seismic interpretation and contouring of Dinantian structures difficult.

2.2. Local geology at Luttelgeest

The LTG-01 well is located on the Luttelgeest carbonate platform which is found on the Texel-Ijsselmeer structural high, a prominent NW-SE trending fault block of mid-Palaeozoic origin (Fig. 1) (Geluk et al., 2007). The southern boundary is made up of a steep fault system, while the northern margin gradually transitions into the adjacent Friesland platform. The Luttelgeest carbonate platform is elongated in the E-W direction, with dimensions of approximately 14 km E-W and 8 km N-S.

The LTG-01 well was drilled to a total depth of 5162 m. The Dinantian carbonates span the depth interval between 4355 and 5123 m, being in total 768 m thick. The LTG-01 core taken in the Dinantian interval comprises massive dark-grey limestones rich in millimetre sized bioclasts, that commonly contain fractures and vugs filled with early sparitic calcite (Fig. 2). The most abundant microfacies association is bioclastic packstone with abundant crinoids and fragments of echinoids, calcareous algae, foraminifera and brachiopods, as seen in the thin section in Fig. 2a. In the lower 120 m, dolomite is intercalated with limestone. Two depositional environments can be recognized from analysing the core and log. The first is a relatively open environment under moderately agitated conditions below the effective wave base, most likely representing the carbonate platform break. The second is a moderate to high-energy subtidal environment above wave base but in conditions of relatively slow sedimentation which usually occur in the inner platform.

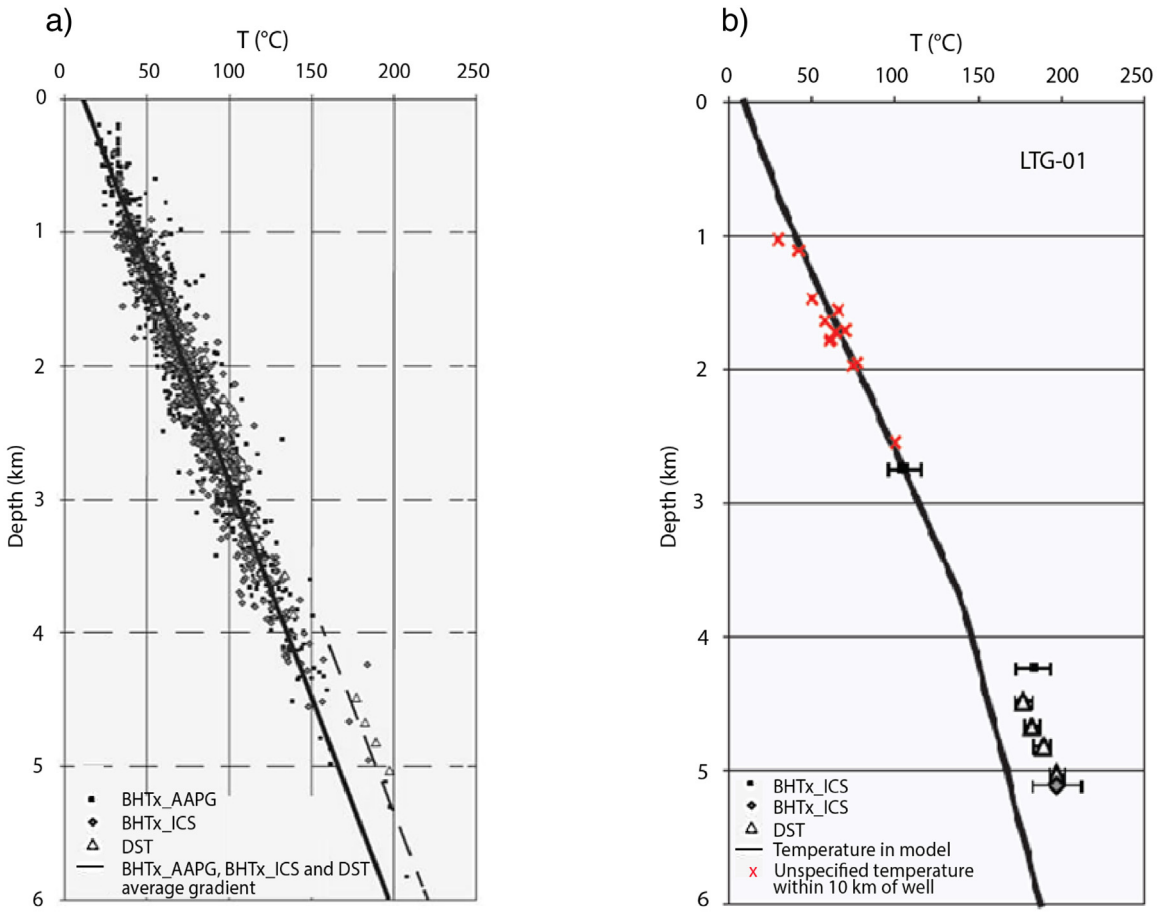

Fig. 4. Temperature vs. depth for the Dutch subsurface. (a) DST and corrected BHT dataset. Dashed black line represents the trend for deeper temperatures. (b) Comparison between the values used as calibration and the modelled temperature for LTG-01. See legend for explanation of symbols (adapted after Bonté et al., 2012).

Various processes during deposition affect the overall geometry of carbonate platforms. A general distinction can be made of platform geometry by considering sedimentological domains including platform interior, margin and slope (Boro et al., 2013). The seismic profile in Fig. 3b shows the relative position of the LTG-01 well, which appears to be situated on the edge of the platform, or platform margin. This is in agreement with other seismic studies of the Luttelgeest platform (e.g. Van Hulten and Poty, 2008).

3. Evidence for convection

The potential for convection in the Luttelgeest platform is evaluated by looking at evidence of convection in temperature data, permeability measurements on cores and by using the Rayleigh number analysis to determine the minimum permeability at which convection could occur in the Luttelgeest platform.

3.1. Temperature

The Netherlands is covered by more than 5000 oil and gas exploration wells, providing valuable information on the thermal state of the Dutch subsurface. Bonté et al. (2012) provides the most recent up-to-date coherent temperature dataset for the Netherlands, adding to it a number of recently drilled wells including LTG-01. In total, the dataset includes 1293 corrected bottom-hole temperature (BHT) measurements distributed over 454 wells and yields an average gradient of 31.3 °C km^{-1} with a mean surface temperature of 10.1 °C (Fig. 4a). There is, however, a sudden shift in the data towards high temperatures at depths greater than 4 km, as indicated by the dashed line in Fig. 4a. These anomalous high values at great depth correspond to the following deep wells: LTG-01, TJM-02, WSK-01 and GLH-01 (See Fig. 1 for locations).

For a better understanding of subsurface temperatures, Bonté et al. (2012) use this up-to-date temperature dataset to calibrate 3D thermal models for the complete Dutch subsurface. Models use a tectonic heat flow method that is based on the varying petrophysical parameters and the transient effects of vertical tectonic motions. The modelling method takes into account not only the well itself, but the closest values around the well in order to calibrate the model (Bonté et al., 2012).

The comparison between the model and the values within a 10 km radius of the LTG-01 well is shown in Fig. 4b (Bonté et al., 2012). The complete dataset for LTG-01 yields a temperature gradient of 39 °C km^{-1}, though contains several intervals of anomalous values. Most notably, within the platform the gradient is nearly 10 °C km^{-1} lower than the Dutch average, whereas above the platform the gradient is roughly 20 °C km^{-1} higher.

The first observation is that between 1 and 4 km, the results show a good fit of the temperature model with the calibration data. In the Noordoospolder area, the low conductivity overlying Silesian shale and coal is thick. The Silesian has an insulating effect, resulting in lower temperatures at the top of the Silesian and higher than average temperatures at the base. In LTG-01 well, the Silesian is reached at 1776 m. The insulating effect is represented by the steep gradient extending down to 3800 m. This is in agreement with the close proximity wells (indicated in red in Fig. 4b).

Another important observation is the major misfit of temperatures deeper than 4 km, which are all higher than the modelled temperatures. There are several different mechanisms that could explain the local thermal configuration, including basal heat flow

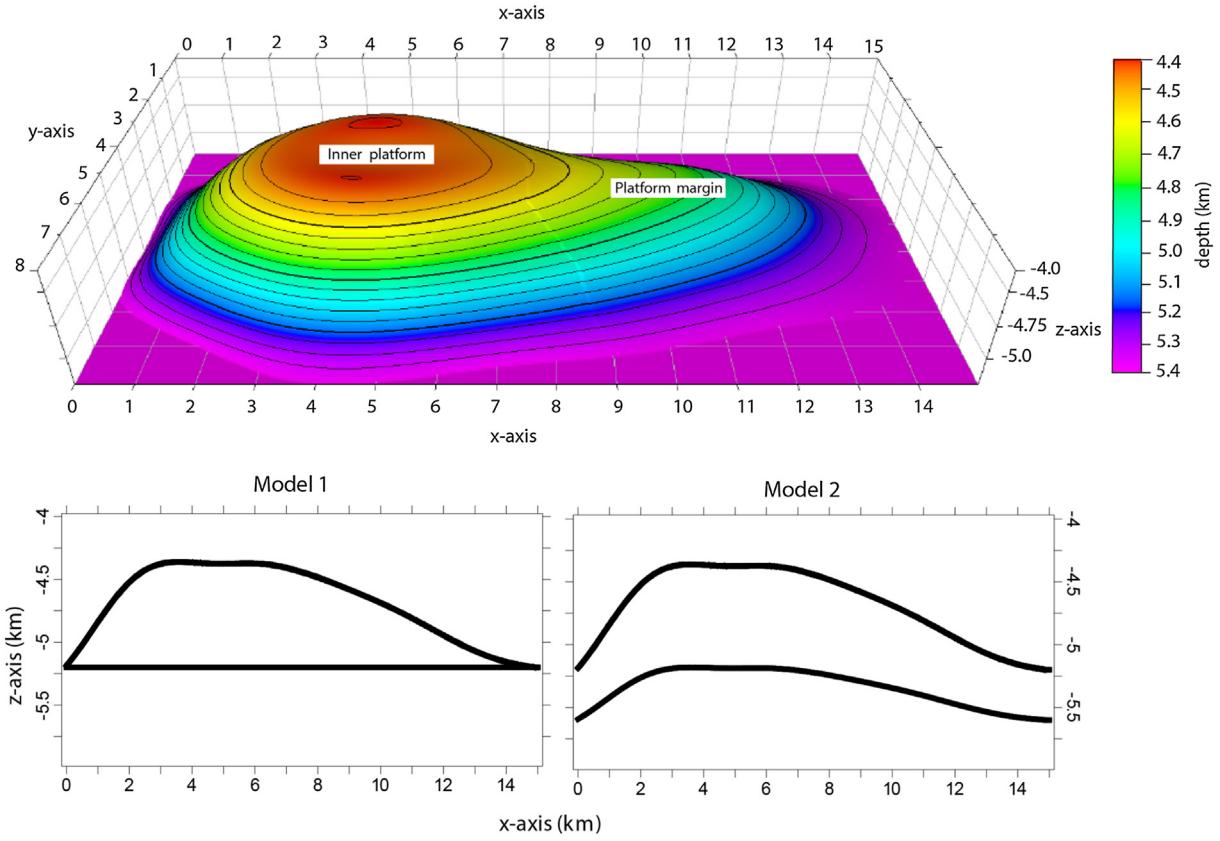

Fig. 5. Geometry of platform. Inner platform and platform margin indicated. Platform is at a depth of 4.4–5.2 km. Bottom: cross sections showing the different geometries in model 1 and model 2.

variation, thermal conductivity contrasts or additional heat generation. For example, higher conductivity may result in heat refraction effects, whereas a thick sedimentary cover may cause an increase in temperatures due to a lower thermal conductivity, known as thermal blanketing. Thermal blanketing effect is well recognized in studies (e.g. Ziegler et al., 1998; Van Wees and Beekman, 2000). Additionally, variation in basal heat flow can cause regional variations in the surface heat flux. A high heat generating body such as a granite intrusion may also cause additional heat generation thereby enhancing the surface heat flow (e.g. Cloetingh et al., 2010).

The conductive model by Bonté et al. (2012) does not give the predicted conductivity structure. Bonté et al. (2012) addresses several different explanations for the thermal anomaly. At the base of their model, the heat flow of the basin fill gives a value of 53 mWm^{-2}. This value is too low to be able to reach the high temperatures required by using coherent thermal conductivity values in the Carboniferous (around 1.7). However, it cannot be ruled out that perhaps the Carboniferous conductivity is high, which could give a refraction effect of the geotherm as seen in the Luttelgeest model. There are simply not enough conductivity measurements to rule it out. Furthermore, while the presence of local heat structures could cause thermal variations spatially, it would not cause a vertical differentiation of the gradient. Further, there have been no recent heat sources nor tectonic processes.

If the model is to fit the measured data from LTG-01, the geothermal gradient would need to increase between 3 and 4 km, and then decrease between 4 and 5 km through the carbonate platform (Fig. 4b). Such a decrease in the temperature gradient is typical of a convective signature resulting from hot upwelling fluid (Guillou-Frottier et al., 2013). In this study, we investigate the possibility that the thermal anomaly at Luttelgeest is due to the occurrence of convective heat transfer in the deep carbonate platform. Thermal convection can cause small-scale thermal anomalies, provided permeability is sufficient.

3.2. Permeability assessment

Permeability was calculated by TOTAL from wirelines pressure tests and reported in the composite log (report accessible from www.nlog.nl)The permeability values range from 10 to 598 mD (10^{-14} to 6 10^{-13} m^2), however several measurements were registered as fair or questionable. Van Oversteeg et al. (2014) calculated the permeability and transmissivity based on mud losses and proposed that there is an interval with fracture permeability between 4550–5150 m. For a reservoir thickness of 600 m, an overall permeability of 6 10^{-14} m^2 was calculated (Van Oversteeg et al., 2014). This value is in accordance with the permeability range inferred from pressure measurements, but should be taken with caution as the permeability is not equally distributed throughout the entire interval of 600 m. For example, between 4800 and 4975 m there is no evidence of permeability.

An overview of the permeability assessment is presented in Table 1. The cuttings description of the composite log states that no visible porosity was encountered. According to Van Hulten and Poty (2008), only a few fracture zones were encountered on bore hole imaging. Van Hulten and Poty (2008) propose that the two fracture zones corresponding with high gamma ray peaks indicate karstified horizons. However, the fact that fracture zones have high gamma ray peaks likely implies argillaceous, clay-rich fracture sedimentation. Furthermore, areas of potential permeability increase can be derived from wireline logs by comparing the neutron porosity and density logs. High neutron porosity and low density indicate areas with increased/present porosity that can be translated to permeability. In fact, several mud losses are encountered in the

Table 1
Overview of results from the permeability assessment of the Dinantian carbonate interval from LTG-01 well.

Source/method	Depth interval	Permeability
Composite well log	Several intervals show signs of increased permeability	
Wireline Pressures	4535–4647 m (100 m)	10–598 mD (10^{-14}–6 10^{-13} m^2)
Rock samples	4378–4473 m (100 m)	0.2–9.6 mD (2 10^{-16}–9 10^{-15} m^2)
Mud loss calculations	600 m	>1D (10^{-12} m^2)

Table 2
Nomenclature for model equations.

Symbol	Name	Unit
Ra	Rayleigh number	–
Ra^*	Critical Rayleigh number	–
k	Permeability	m^2 or mD
k_{min}	Minimum permeability for convection	m^2
α	Volumetric thermal expansion coefficient	$°C^{-1}$
ρ	Bulk Density of porous rock	kg m^{-3}
ρ_f	Fluid density	kg m^{-3}
ρ_0	Reference density	–
C	Bulk Specific heat capacity of porous rock	J kg^{-1} K^{-1}
C_f	Specific heat capacity of fluid	J kg^{-1} K^{-1}
C_h	Bulk hydraulic storage capacity of porous rock	m^3 Pa^{-1}
g	Gravitational acceleration	m/s^2
H	Total thickness of the aquifer	m
T	Temperature	°C
t	Time	s
P	Pressure	Pa
ΔT	Temperature difference across layer	°C
μ	Fluid viscosity	Pa s
λ	Thermal conductivity	W m^{-1} K
Q	Source term	m^3 s^{-1}

well; one at 4450 m, six between 4575 and 4700 m, one at 4775 m and two between 4975 m and 5025 m, which points to permeability streaks that are probably related to fractures. The combination of neutron porosity and density indicates porous intervals around 4500 m, between 4570 and 4600 m, and between 4770 and 4800 m.

3.3. Permeability from Rayleigh number analysis

Assuming that thermal convection is able to explain the abnormally low thermal gradient within the Luttelgeest platform at well LTG-01, the rationale of Horton and Rogers (1945) and Lapwood (1948) can be followed to find the minimum required permeability values for convection. The Rayleigh number is a non-dimensional number that includes characteristics of the porous medium, thermodynamic properties of the fluid and a vertical temperature difference. In a homogeneous, isotropic porous medium saturated by a single-phase fluid, the Rayleigh number is defined as

$$\mathrm{Ra} = \frac{k\alpha\rho^2 c_p g H \Delta T}{\mu\lambda} \quad (1)$$

See Table 2 for nomenclature. The critical Rayleigh number for onset of convection is calculated from linearized governing equations (Lord Rayleigh, 1916). If Ra is above the threshold value of the system, known as the critical Rayleigh number (Ra^*), convection is expected to occur. For a horizontal, homogeneous isotropic porous medium bounded from above and below by fixed temperature conditions, Ra^* is $4\pi^2$.

Using Ra^*, Eq. (1) can be rewritten to constrain the minimum required permeability (k_{min}):

$$K_{min} = \frac{Ra^* \mu \lambda_e}{\left(\rho C_p\right) \rho g \alpha \Delta T H} \quad (2)$$

For the parameter values, site specific values from LTG-01 well are used for the temperature difference and the height of the convective layer. Furthermore, temperature dependent relationships are used for density and fluid dynamic viscosity, as provided by Holzbecher (1998) (see Section 4.2). By means of the Rayleigh number analysis using the temperature range of the carbonate platform (182–213 °C) and a thickness of 800 m, the theoretical minimum permeability for convection is 1.9 10^{-14} m^2.

While the theoretical Rayleigh number analysis can be a useful tool in determining the conditions necessary for the onset of convection, it does ignore several important factors, such as the heterogeneous nature of fluid and rock properties of the reservoir (Nield and Bejan, 2013). In addition, the critical Rayleigh number applies to a specific set of conditions, including initial and boundary conditions and the geometry of the layer. This study assumes the carbonate platform is uniformly heated from below and is a perfect conductor. Changing the lower thermal boundary condition may result in smaller values for Ra^* (Bjørlykke et al., 1988).

Moreover, conductive heat transfer along the sides of the platform is likely to play a role in the overall physical state and stability of the convective system. Murphy (1979) highlighted on the fact that heat transfer between fluid in the permeable layer and surrounding rock is exceptionally stable. Tournier et al., (2000) demonstrated that this blanketing effect of thermal gradients across vertical walls by conduction might result in delayed onset of convection. Though the conjectures of both Murphy (1979) and Tournier et al. (2000) were related to studies on the onset of convection in vertical fault planes, the concept can be applied to any confined, fluid saturated medium where convective fluid flow is occurring. Thus, assuming that only convective heat transfer is occurring in the system is a significant simplification to the model.

4. Methods

4.1. Governing equations

The numerical study of thermal convection in permeable and porous media involves the coupling of heat transfer and fluid flow equations that incorporate realistic fluid and rock properties. In a Eulerian reference framework, the heat equation is written as

$$\rho c \frac{\partial T}{\partial t} = \nabla \cdot (\lambda \cdot \nabla T) - \vec{v} \cdot \nabla T \quad (3)$$

See Table 2 for nomenclature. The advective velocity can also be a result of fluid flow inside pores or fractures which can strongly affect the thermal distribution (e.g. Guillou-Frottier et al., 2013; Cherubini et al., 2014). The fluid velocity is resolved from solving the Darcy flow equation:

$$c_h \frac{\partial P}{\partial t} = \nabla \cdot \left(\frac{k}{\mu} \left(\nabla P + \frac{\left(\rho_f - \rho_0\right)}{\rho_0} g \nabla z \right) \right) + Q \quad (4)$$

See Table 2 for nomenclature. Through solving the pressure field in Eq. (4), the velocities can be determined as

$$\rightarrow v_f = \frac{k}{\mu} \left(\nabla P + \frac{\left(\rho_f - \rho_0\right)}{\rho_0} g \nabla z \right) \quad (5)$$

And can be incorporated in (Eq. (3)) by adopting:

$$\vec{v} = \varphi \frac{\rho_f c_f}{\rho c} \rightarrow v_f \quad (6)$$

4.2. Petrophysical and fluid properties

The following properties are considered temperature dependent and have been defined here. Laws are based on experimental data measured on pure water between 100 and 300 °C (Holzbecher, 1998). Under single-phase conditions, the following polynomial trend has been chosen for temperature dependent density

$$\rho = 1758.4 + 10^{-3}T - \left(4.8434 \times 10^{-3} + T\left(1.0907 \times 10^{-5} - 9.8467 \times 10^{-9}T\right)\right) \quad (7)$$

where T is in K and ρ in kg m^{-3}. For the relationship between temperature and fluid dynamic viscosity, the law adapted by Rabinowicz et al. (1998) is used:

$$\mu = 2.4141 \times 10^{-5} \times 10^{\frac{247.8}{T-140}} \quad (8)$$

where T is in K and μ in kg m^{-1} s^{-1}.

4.3. Geometry and boundary conditions

Three-dimensional coupled fluid and heat transport models are simulated using a numerical solver developed in a Java programming language. The equations are solved in a 3D cellular model. A 3D model of the platform was constructed with grid resolution of 100 × 100 m in the x and y directions and 10 m in the z direction at platform depth level and xx m in the z direction elsewhere A sensitivity analysis was performed only within platform, using a larger mesh size (200 × 200 × 10 m) as well as a smaller one (50 × 50 × 10 m). There is no discrepancy in the temperature nor the convection cell width between the different mesh sizes. The top of the platform is at a depth of 4.4 km and base at 5.2 km, resulting in a thickness of 800 m. The model domain extends from the surface to below the base of the platform down to a depth of 6 km. The platform extends 14 km and 8 km in the x and y directions, respectively. This results in a total 896,000 for the 100 m resolution model and 224,000 and 358,4000 grid cells for the 200 and 50 m resolution models, respectively. Temperature at the top of the model is 10 °C and 244 °C at the bottom reflecting a linear thermal gradient of 39 °C km^{-1}. This gradient is chosen based on the calculated average gradient from the LTG-01 temperature data. All boundaries of the platform are impermeable, defining a closed system with no sources or sinks for the fluid. Lateral boundaries are thermally insulating. Rock thermal properties are assumed to be uniform for the entire model.

Experiments begin with an initial perturbation to the conductive temperature field by injecting cold fluid into the platform. If the system is unstable ($Ra < Ra^*$), a perturbation to the diffusive regime will grow and instability will occur, generating convection cells (Weatherill et al., 2004). An instability in a real system could be caused, for example, by lateral contrasts in the temperature gradient, for example caused vertical tectonic movement. A sensitivity analysis was carried out with regard to the location of perturbation and its magnitude relative to the background temperature. While convection cells do initially develop from the location of perturbation, at pseudo steady-state the system evolves into the same convection cell pattern with matching wavelengths, regardless of the location of perturbation. During computation, the initial conductive field evolves towards steady-state convection within a few thousand years, therefore simulations run for 500 k years.

The prediction of convective flow patterns necessitates the use of 3D numerical modelling to allow for a more accurate specification of platform geometry, which has a significant control on convection cell development. Indeed, simple 2D models of thermal convection show that. The introduction of a third dimension results in a complex polyhedral structure which cannot develop in 2D. Two-dimensional models represent an oversimplification, marked by convective instabilities which occur in the form of longitudinal square rolls, but are still commonly used in numerical studies, despite several studies demonstrating that 2D and 3D models of convection can produce significantly different results with flow velocities of 2D models one order of magnitude lower than in the 3D case (e.g. Kühn et al., 2006). This study presents convective patterns which result from 3D numerical models of thermal convection.

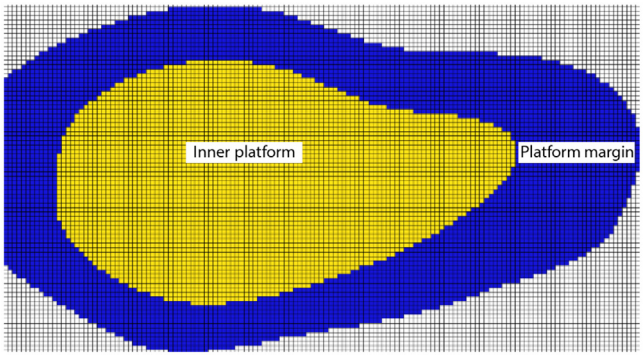

Fig. 6. Top view of the platform showing the permeability differentiation between platform margin and inner platform areas. The platform margin is assigned a higher permeability. See Table 4 for permeability values.

4.4. Model scenarios

We begin with several convective flow simulations using a constant, homogeneous permeability. In doing so, two platform geometries are tested. The first geometry, referred to as model 1, is characterized by a flat platform base, where the thickness of the inner platform is 800 m. In the second geometrical configuration (model 2) the shape of the platform top remains the same, however the base of the platform is curved upwards. In order to keep the thickness of the inner platform at 800 m, the thickness of the margins is increased by 400 m, extending down to 5600 m depth at the platform margin. Fig. 5 provides an overview of the model geometries.

In carbonate platforms it is common for fractures to be less common in the inner platform and prominent in the outer platform to rim/slope area as seen in international analogues such as the Tengiz and Kashgan platforms in Kazakhstan (Collins et al., 2006; Kenter et al., 2002). Therefore, in the second set of convective flow simulations we investigate the effect of the permeability structure on convective flow. The margins of the platform have increased permeability, while the inner platform region is assigned a lower permeability. Fig. 6 depicts the differentiation between the inner platform and the platform margin. We also present two cases which address the effect of an anisotropic permeability field.

5. Results

5.1. Platform geometry sensitivity

A system is said to be in steady state convection once a constant fluid velocity is reached. The convection cell width is assessed by measuring the distance between each thermal high and its closest neighbor and halving it. As discussed in Section 3.3, the theoretical minimum permeability required for convection is 1.9 10^{-14} m^2. A range of permeability values are tested in numerical simulations, and by doing so we find the modelled minimum permeability is 1.7 10^{-14} m^2. Here the results for two permeability values are presented, 2 10^{-14} m^2 (subscript a) and 6 10^{-14} m^2 (subscript b), which are taken uniform over the platform and applied to both geometric scenarios (models 1a,1b, 2a,2b). An overview of the scenarios and the results is provided in Table 3.

Table 3
Numerical model results at end of simulation for models 1 and 2. T is the maximum temperature obtained along the axes of upwelling. Tc is the temperature without convection. T–Tc is the overall temperature enhancement relative to the conductive profile.

	Permeability (m^2)	T (°C) at 4.4 km	T–Tc (°C) at 4.4 km	Cell width (km)	Fluid velocity ($m\,yr^{-1}$)
1a	$2\,10^{-14}$	192	11	1.1	1.3
1b	$6\,10^{-14}$	197	16	1.0	1.9
2a	$2\,10^{-14}$	196	15	1.3	1.8
2b	$6\,10^{-14}$	203	22	1.3	2.6

5.1.1. Convection cell structure

Results show that the development and number of convection cells is very much a time dependent process. The first sign of convective motion appears after 8k years in the form of longitudinal rolls forming from the location of perturbation. Longitudinal rolls fill the domain, increasing in width until eventually transforming into a more complex polyhedral structure within 50k years in all models. The system gradually develops into a distinct convective patter with alternating up-flows and down-flows, reaching steady-state convection after approximately 180k years in model 1a and 160k in model 1b.

Model 1a relaxes into a steady-state 8 cell convection pattern (Fig. 7a). This structure is characterized by four dominant upwelling plumes: two circular plumes in the thickest part of the platform, and two elongated plumes closer to the platform margin. The average convection cell width is 1.1 km. In cross-section view the upwellings are represented by significant uplift in the isotherms, all of comparable magnitude. Model 1b relaxes into a marginally more complex steady-state convection pattern (Fig. 7b). As in model 1a, the upwelling plumes are concentrated in the thickest part of the platform. The structure is characterized by four elongate polyhedral shapes. The average convection cell width is 1 km. The fluid circulates at an average velocity of 1.3 m yr^{-1} and 1.9 m yr^{-1} in model 1a and 1b, respectively. These values are in agreement with other studies on thermal convection in permeable basement and sedimentary layers (e.g. Guillou-Frottier et al., 2013; Schilling et al., 2013; Sheldon et al., 2012).

In models 2a and 2b, the base geometry of the platform changes from flat to upward curving, tracing the same shape as the top of the platform. The thickness at the margins is increased by 400 m in order to keep a constant thickness of 800 m in the platform interior. The development of convection cells follows that of model 1, where the first sign of convective motion takes the form of longitudinal rolls before 10k years. Steady-state convection is reached earlier, at 140k and 150k years in 2a and 2b, respectively. Model 2a relaxes into a steady-state structure that is a combination of circular and elongated shaped upwellings (Fig. 8a), whereas model 2b is dominated by a more circular upwelling pattern with an increased number of convection cells (Fig. 8b). Both models have an average cell width of 1.3 km. The fluid velocity at steady-state is approximately 1.8 m yr^{-1} and 2.6 m yr^{-1} in model 2a and 2b, respectively.

5.1.2. Temperature

The circulation of fluid has a major impact on the geothermal gradient and temperature patterns. Fig. 9 shows how convective fluid flow effects the temperature field in models 1 and 2, depending on the geometry and permeability of the platform. The measured temperature values from within the platform in well LTG-01 have been added for reference. Geothermal gradients have been taken along the axis of three points in each model: downwelling, mixing zone and upwelling. This represents how the shape of the gradient differs depending on the direction of fluid circulation, be it upwards or downwards.

At the top of the platform, large positive temperature anomalies are produced in areas of upwelling, whereas negative anomalies are present in zones of down-flow. In models 1a and 1b, the temperature peaks at around 192 °C and 197 °C in the center of upwelling areas, while the temperature is only 186 °C and 189 °C in zones of down-flow, respectively (Fig. 9a-b) In models 2a and 2b, the temperature is elevated to 196 °C and 203 °C in upwellings and reduced to 176 °C and 181 °C in down-flows (Fig. 9c–d).

The next observation is the overall shape of the geothermal gradients. Along the axes of upwelling, the gradient is steepest which results in relatively low gradients through the platform. The gradient is as low as 13 °C km^{-1} in model 2b, where the platform has both a large permeability and thickness. Consequently, the largest temperature enhancement (22 °C) at the top of the platform is also present in model 2b. Along the axes of downwelling, convective fluid flow causes the geothermal gradient to lower by 10–15 °C km^{-1}. In models 1a and 1b, the average geothermal gradient within the platform is 28 °C km^{-1} and 25 °C km^{-1}, respectively. By changing the base geometry from flat to curved, the average geothermal gradient decreases to 22 °C km^{-1} and 18 °C km^{-1} in models 2a and 2b. As models have matching thermal boundary conditions, the temperature oscillates around the same temperature (200 °C) at mid-depth.

The final observation is the fit of the modelled geothermal gradients with measured temperature values from well LTG-01. Looking at the overall trend of the modelled temperatures, it appears, with exception to the gradient along the axes of downwelling, that the models overestimate temperatures in the top and intermediate depth levels of the platform. The modelled and measured temperatures are comparable, but it is not a superimposed fit. While the temperature data set from the LTG-01 well does suggest that the average gradient is elevated with respect to the Dutch average gradient of 31 °C km^{-1}, it appears that applying a gradient of 39 °C km^{-1} causes an over enhancement of temperatures once convection stabilizes within the carbonate platform reservoir.

We therefore adjust the boundary conditions such that the gradient is no longer elevated, taking a closer look at the local nature of the thermal anomaly within the platform (Fig. 10). The permeability has also been scaled, as the minimum permeability required for convection is now higher due to the decrease in ΔT. (see Eq. (2)). This correction to permeability can be performed as the permeability is within the same order of magnitude. The temperature enhancement relative to the conductive profile is similar to the previous models. As the geothermal gradient is now lower, the maximum temperatures attained within regions of upwelling are lower, ranging from 182 °C in model 1a to 192 °C in model 2b. Not only are these temperatures more comparable with the measured temperature values, but the modelled geothermal gradients along axes of upwelling are also a better fit with the measured gradient at LTG-01 well.

5.2. Permeability structure sensitivity

In the second series of numerical experiments denoted as model 3, we test how different mechanisms and processes affect the development of convection by investigating the sensitivity of the permeability structure (refer to Fig. 6 for permeability setup). An overview of the cases that are tested is provided in Table 4. Results

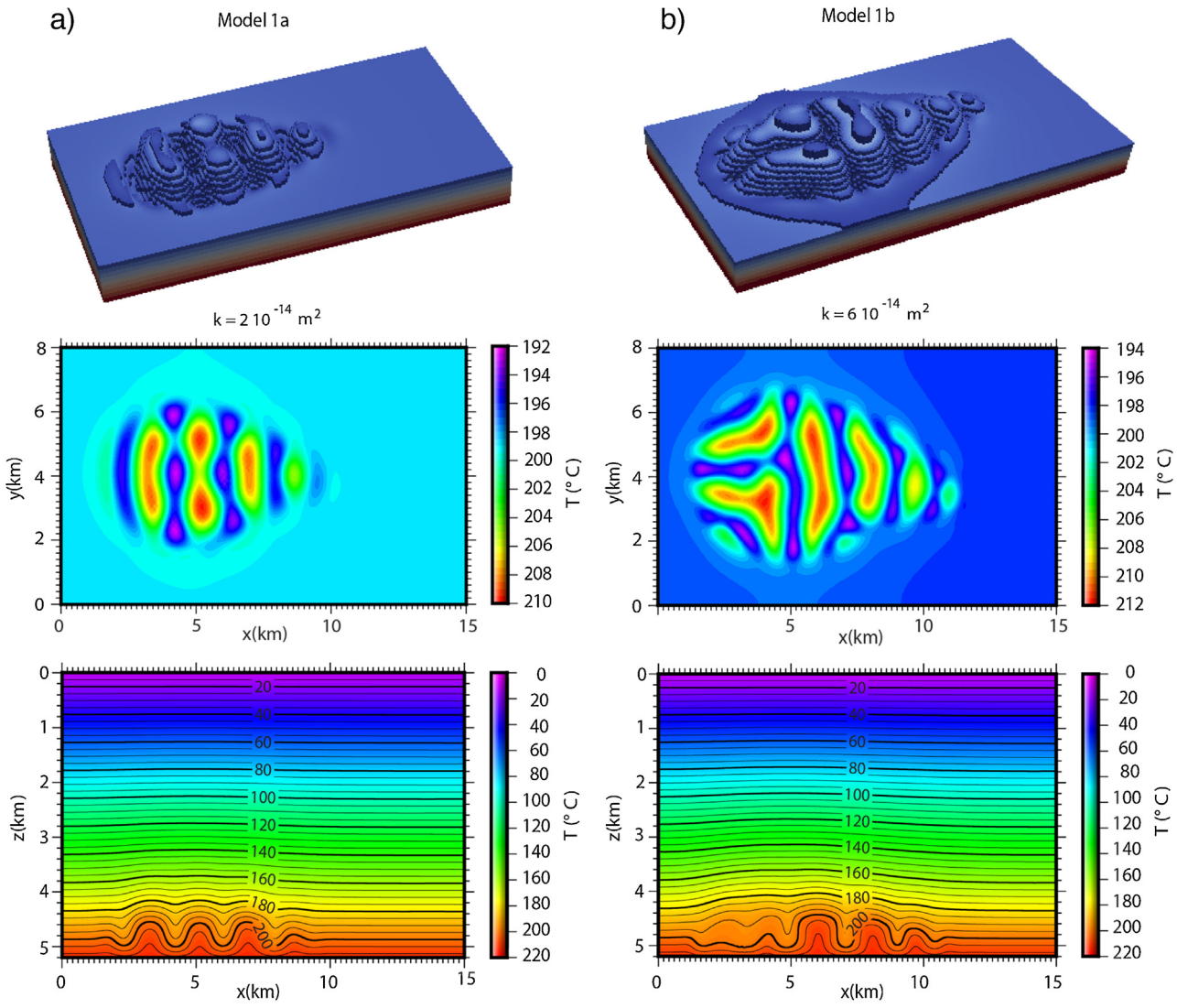

Fig. 7. (a) Results for model 1a. (b) Results for model 1b. Top: 3D view of the modelled temperature field at the top of the platform (4.4 km). Vertical exaggeration = 2. Middle: Temperature on the horizontal plane at z = 4.8 km. Note different temperature scale between (a) and (b). Bottom: Cross section at y = 4 km.

are presented in Fig. 11. The structure of convection is discussed first, followed by a summary of the resultant temperature fields.

The first permeability structure tested, model 3a, is one dominated by a permeability of 6 10^{-14} m^2 in the margin and 1 10^{-14} m^2 in the inner platform. Note that the inner platform permeability is below the permeability threshold for convection. Therefore, flow is constricted to the platform margin. Interesting to note is that the initial convection structure takes on the form of longitudinal rolls throughout the entire platform. However, with time flow dissipates in the inner platform as the fluid at depth is surrounded by less permeable rock and unable to facilitate flow. The steady-state structure is dominated by a circular upwelling platform within the platform edges. Again we see that the largest upwellings are concentrated in the thickest marginal area.

By increasing the inner platform permeability above the threshold to a value of 2 10^{-14} m^2 and keeping the margin permeability at 6 10^{-14} m^2 there is a slight modification in the steady-state convection cell structure. An elongated shaped upwelling appears in the inner platform, however the largest upwellings remain concentrated in the platform margins. The temperature enhancement in both are similar (model 3a–b in Fig. 11). The next two cases (model 3c–d in Fig. 11) test the effect of introducing

Table 4
An overview of the four cases used in the permeability structure sensitivity tests. Kx,y is the permeability in the horizontal direction. Kz is the permeability in the vertical direction. T is the maximum temperature obtained along the axes of upwelling. Tc is the temperature without convection. T–Tc is the overall temperature enhancement relative to the conductive profile.

Model	Inner platform		Platform margin		T (°C) at 4.4 km	T–Tc (°C) at 4.4 km
	Kx,y	Kz	Kx,y	Kz		
3a	10	10	60	60	190	9
3b	20	20	60	60	194	13
3c	15	60	30	60	188	7
3d	20	100	60	100	196	15

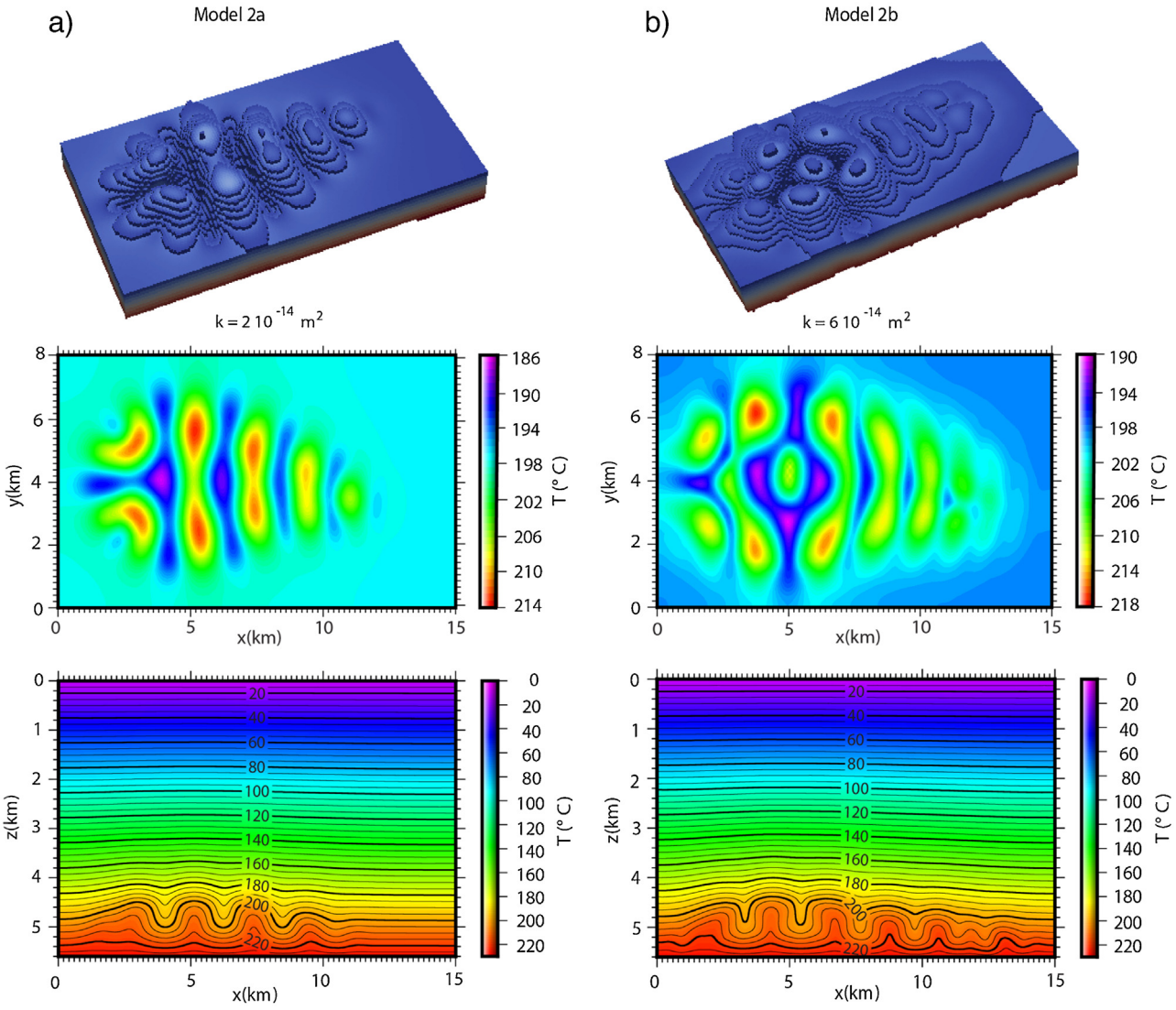

Fig. 8. (a) Results for model 2a. (b) Results for model 2b. Top: 3D view of the modelled temperature field at the top of the platform (4.4 km). Vertical exaggeration = 2. Middle: Temperature on the horizontal plane at z = 4.8 km. Note different temperature scale between (a) and (b). Bottom: Cross section at y = 4 km.

an anisotropic permeability field. As in the first two cases, the platform margin is given a higher permeability than the inner platform, however now the vertical permeability is increased with respect to horizontal. As the vertical permeability is increased, the width of the convection cells decreases. Thus an increase in anisotropy causes upwellings to become more numerous, as they take on a more complex polyhedral shape (model 3d in Fig. 11).

As in models 1 and 2, the geothermal gradients have been measured along three axes (a downwelling, mixing zone and upwelling) (Fig. 12). The first observation is that the modelled temperature values have a better fit with the measured data. Whereas in models 1 and 2 the temperatures are overestimated in the top to middle platform, in model 3 there is a close fit with the measured data particularly within mixing zones. The temperature enhancement within regions of upwelling is lower than in models 1 and 2, ranging from 7 °C in model 3c to 15 °C in model 3d. The lowest gradient is therefore observed in model 3d of 18 °C km^{-1}, which is still noticeably larger than the 13 °C km^{-1} gradient in model 2b. The average geothermal gradient within the platform is 28 °C km^{-1} and 26 °C km^{-1} in models 3a and 3c, and lower values of 25 °C km^{-1} and 23 °C km^{-1} in models 3b and 3d, respectively.

While model 3 does have a better fit with the measured data, the modelled geothermal gradients remain elevated above the platform and at the base of the model due to the set boundary conditions. Therefore following the procedure in models 1 and 2, the boundary conditions are adjusted so that gradient is no longer elevated. Results are presented in Fig. 13. As seen in models 1 and 2, the temperature enhancement at the top of the platform relative to the conductive profile is comparable. The geothermal gradient along axes of upwelling range from 25 °C km^{-1} in model 3a to 18 °C km^{-1} in model 3b. The fit with measured data extends to the base of the platform (at depths greater than 5.2 km), where there is no significant elevation in the geothermal gradients with respect to the measured gradient (black curve). For example, the gradient along the axis of mixing zone in model 3b in Fig. 13 is roughly 10 °C km^{-1} lower than the average Dutch gradient, matching the dataset for the Dinantian carbonates in well LTG-01.

6. Discussion

Three-dimensional numerical models of thermal convection have shown that temperature anomalies of more than 15 °C, consistent with measured data, can easily develop within permeable

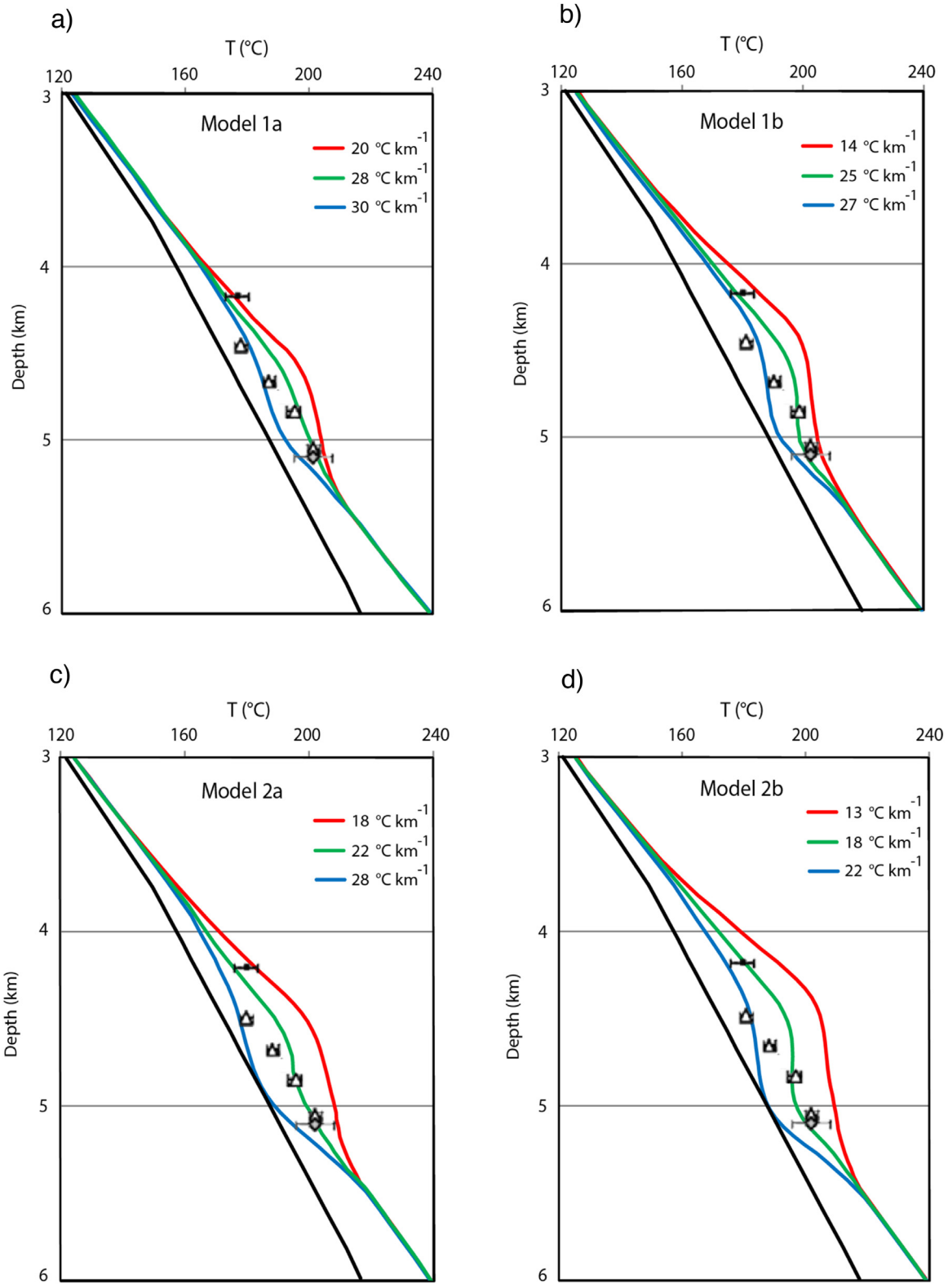

Fig. 9. Modelled temperature-depth profiles along three axes: upwelling (red curve), mixing zone (green curve) and downwelling (blue curve) in models 1 and 2. Measured temperature data from LTG-01 has been included for comparison. Black curve represents measured geothermal gradient. See Fig. 4 for explanation of symbols. (For interpretation of the references to colour in this figure legend, the reader is referred to the web version of this article.)

zones in the Luttelgeest platform. This study argues that the vertical variation of thermal gradient observed within the Luttelgeest carbonate platform cannot be justified by thermal conductivity changes with depth alone, but rather it is evidence of thermal convection.

The Luttelgeest carbonate platform is characterized by intervals of increased fracture permeability, as suggested by wireline

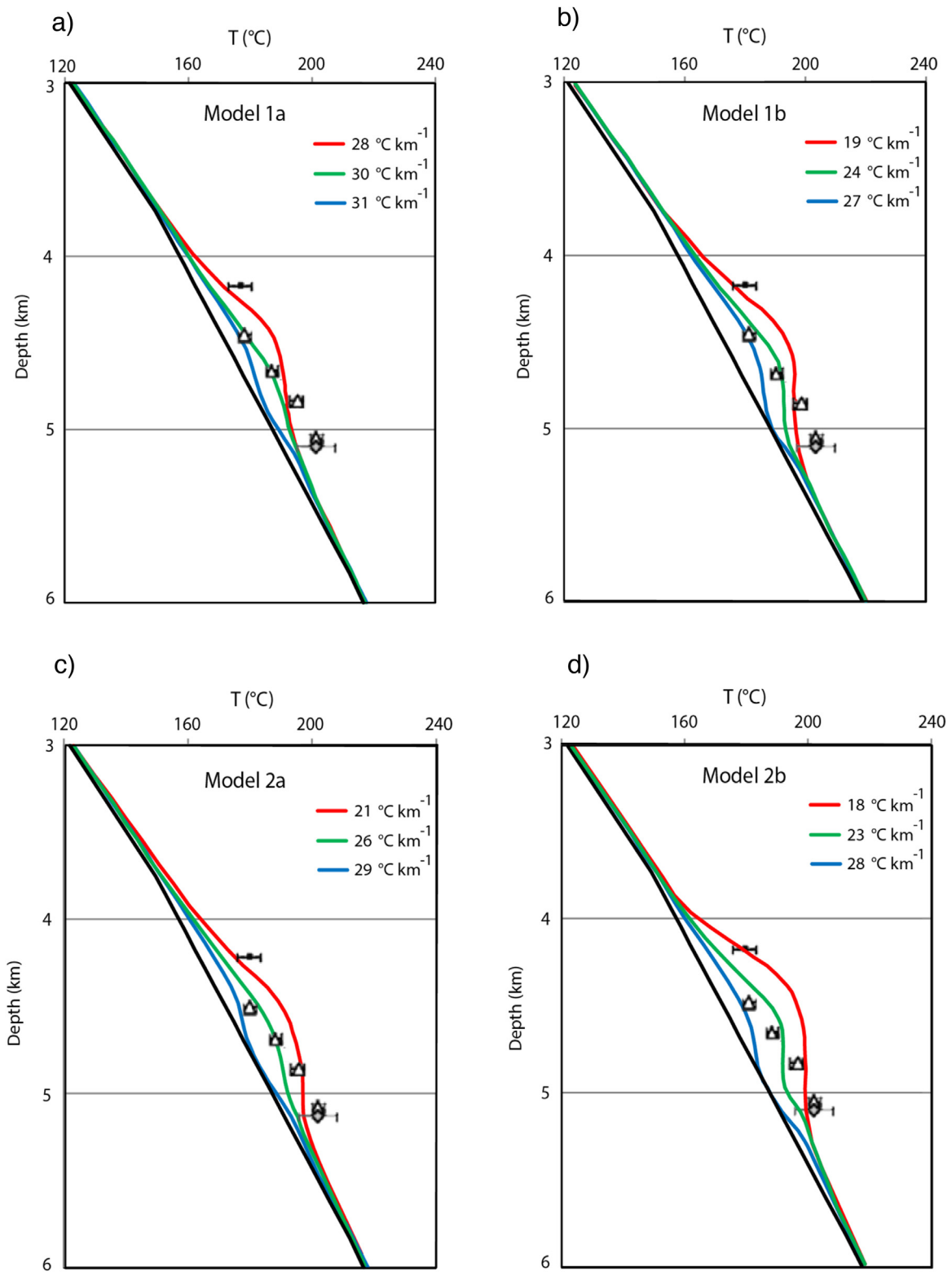

Fig. 10. Modelled temperature-depth profiles along three axes: upwelling (red curve), mixing zone (green curve) and downwelling (blue curve) in models 1 and 2 for a non-elevated gradient. Measured temperature data from LTG-01 has been included for comparison. Black curve represents measured geothermal gradient. See Fig. 4 for explanation of symbols. (For interpretation of the references to colour in this figure legend, the reader is referred to the web version of this article.)

pressure measurements, intervals of high gamma ray and neutron density separation in wireline logs, analysis of mud losses and observations from core samples. Van Oversteeg et al. (2014) proposes that there is a 600 m interval of increased fracture permeability of 6 10^{-14} m^2 between 4150 and 5150 m. However, permeability is not equally distributed throughout the entire platform.

The minimum permeability calculations from the Rayleigh number analysis confirms the potential for free convection. A minimum permeability of 1.9 10^{-14} m^2 is consistent with the per-

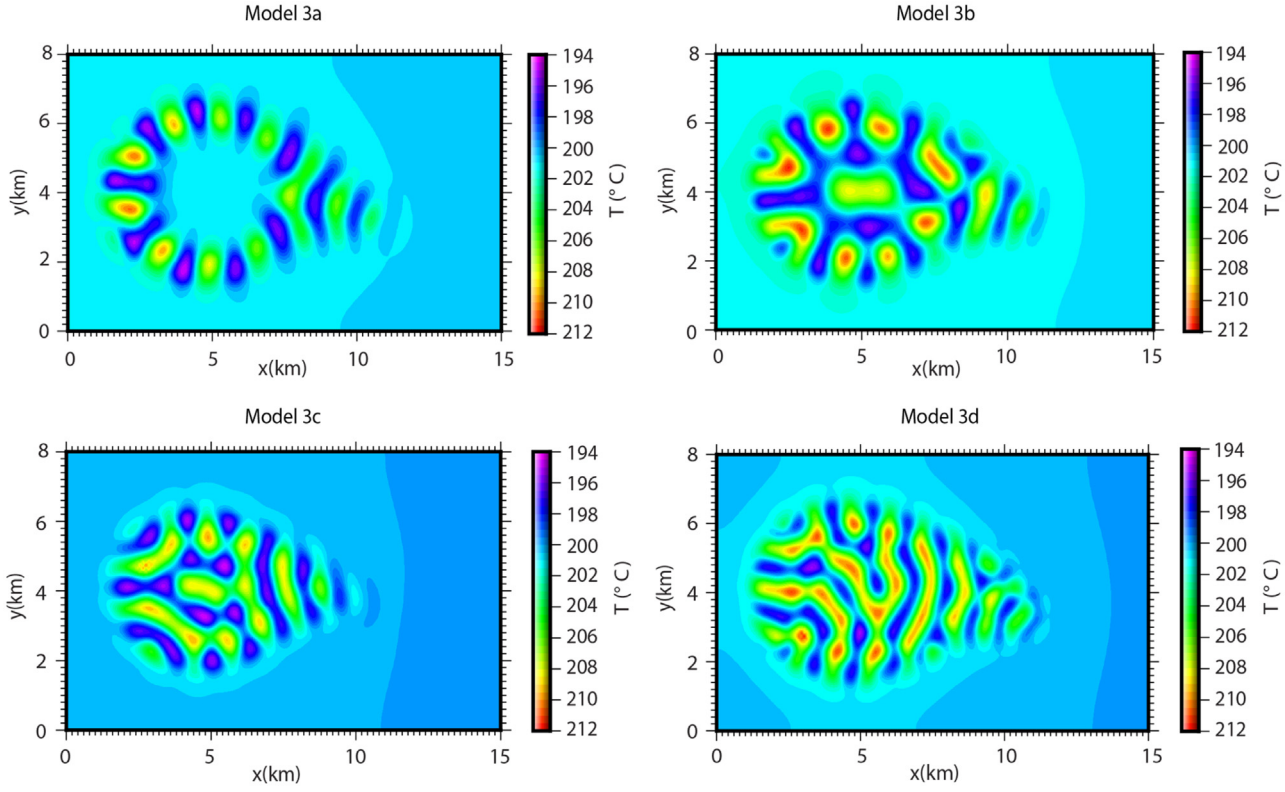

Fig. 11. Temperature on the horizontal plane at z = 4.8 km showing the effect of the permeability structure on convective patterns. For description of each model, see Table 4.

meability calculations derived from the well log and core samples. Compared to other studies, this value is rather large. Pasquale et al. (2013) found for a deep carbonate aquifer of the eastern sector of the Po Plain the minimum permeability to be 3.0 10^{-15} m^2. However, the reservoir considered in this study is significantly thicker (5 km), while the Luttelgeest platform only has a thickness of 800 m. Guillou-Frottier et al. (2013) considers a permeability in the order of 10^{-15} when studying the effect of permeability on convective patterns in the Soultz-sous-Forets region. Again, the layers in question are substantially thicker than this study (4 km). Furthermore, as noted in the permeability assessment, it is likely that there are smaller intervals of increased fracture permeability where the flow is concentrated, for example between 4550 and 5150 m (see Section 3.2). The permeability is also likely to be higher on the margins of the platform than in the inner platform region. The data from Luttelgeest shows that the permeability may be as high as 1 10^{-13} m^2. At this depth interval, a permeability value this large only requires a reservoir thickness of 150 m to facilitate flow.

Numerical model results highlight some important aspects of convection in the Luttelgeest carbonate platform. First, the modelled minimum permeability for convection is 1.7 10^{-14} m^2, which is remarkably close to the theoretical value considering the number of assumptions in the analysis (i.e. ignores the heterogeneous nature of fluid and rock properties and the salinity effects on water density and viscosity). Second, the development of convection cells is a time-dependent process. Convection cells grow from the location of instability at a rate depending on the system Rayleigh number. Third, the preferred initial form consists of multiple longitudinal rolls until 40–50k years, at which point a new structural mode is preferred. At steady-state, the shape of upwellings vary between circular and elongate. The structural development during transition to steady-state differs depending on the system permeability and reservoir thickness. Fourth, permeability heterogeneity controls the onset of convection and instabilities. The shape and location of convection cells in real reservoirs are likely controlled by geometric features such as faults and undulations in the top and bottom surfaces of the reservoir. In fact, three-dimensional convective patterns and preferred convective wavelengths are highly sensitive to lateral dimensions of the permeable zone, and thus three-dimensional numerical modelling reveals new fluid patterns that are not observable in two dimensions, such as the occurrence of hexagonal type convection patterns and complex 3D polyhedral shapes.

In summary, the models which take into account the geometric features of the platform and a realistic permeability structure can explain the thermal anomaly at LTG-01. Using a geometrical configuration based on evidence from seismic studies of Luttelgeest allows for the model to incorporate the effect of the platform slope on thermal developments. Carbonate platforms are heterogeneous in nature, as they form on different scales and in different geometries. This is because platforms form under a variety of sedimentological conditions. The platform margin and platform interior often differ in permeability structure, with the margins of the platform being more heterogeneous in nature and with dissolution enlarged fractures (Boro et al., 2013). Karstification tends to be more effective on the platform rims, and fracture networks tend to be more pronounced on platform edges (eg. Boro et al., 2013). As seen in models 2a and 2b, zones of upwelling favour the combination of platform margin and areas of sufficient thickness. In fact, thermal features are predominately controlled by thickness and the permeability structure of permeable zones. Anomalies are more developed where the permeable carbonate platform is sufficiently thick.

The temperature enhancement that occurs in convective upwellings is critically dependent on the aquifer thickness, permeability structure and geothermal gradient (see Tables 3 and 4). The numerical results indicate that a temperature as high as 203 °C could be reached at 4.4 km depth for a reservoir which has a

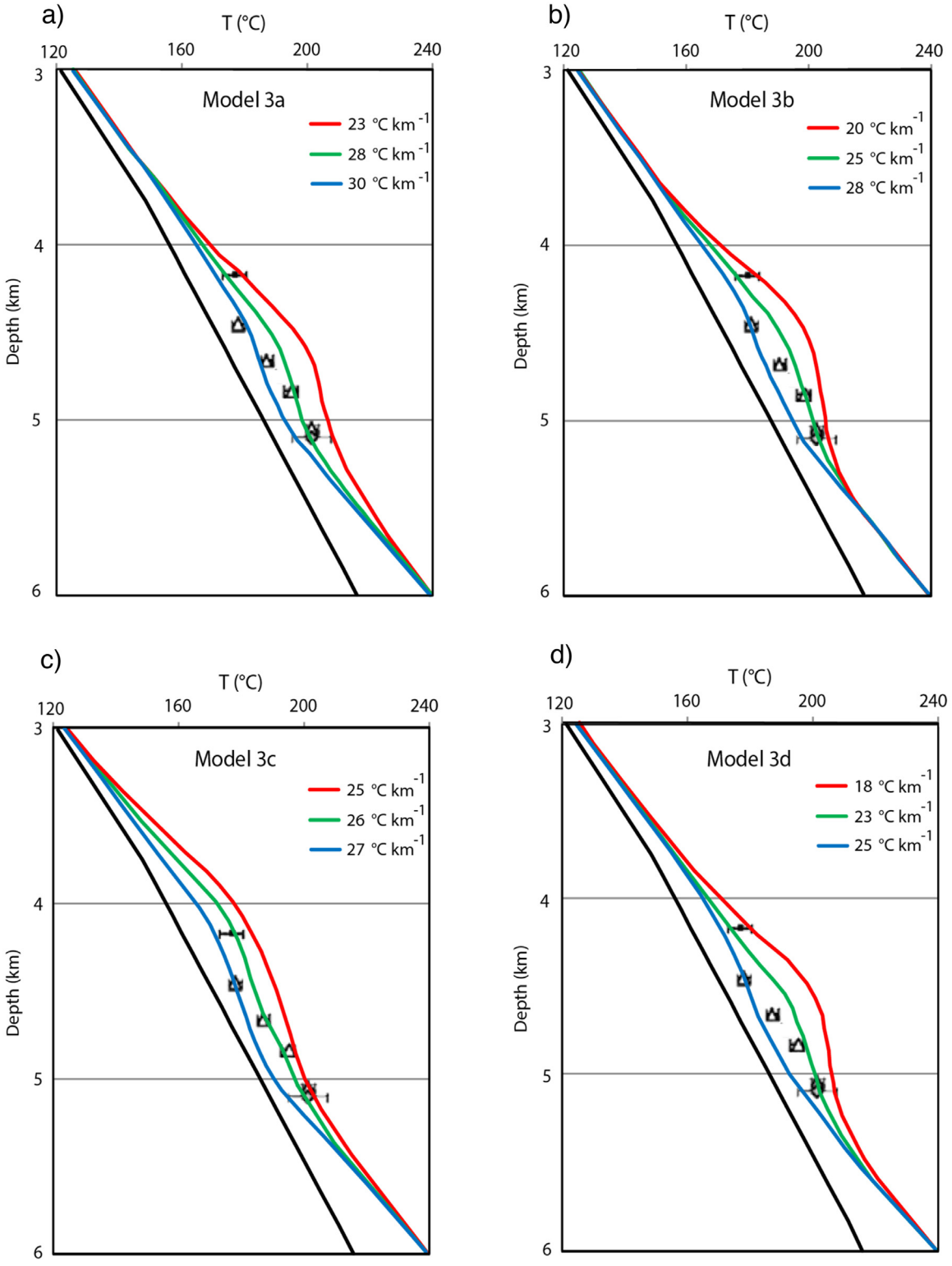

Fig. 12. Modelled temperature-depth profiles along three axes: upwelling (red curve), mixing zone (green curve) and downwelling (blue curve) for model 3. Measured data from LTG-01 has been included for comparison. Black curve represents measured geothermal gradient. See Fig. 4 for explanation of symbols. (For interpretation of the references to colour in this figure legend, the reader is referred to the web version of this article.)

geothermal gradient of 39 °C km^{-1}, a permeability of 6 10^{-14} m^2, an inner platform thickness of 800 m and platform margins extending down to 5.6 km (model 2b). This contrasts the situation in model 1a, where the permeability is 3 10^{-14} m^2 and the platform margin is thinner, resulting in a temperature of 192 °C at the top of upwelling regions. The temperature enhancement in convective upwellings can range from 7 °C in model 3c to 22 °C in model 2b. Even when the geothermal gradient is lowered, the overall temperature enhancement relative to the conductive profile can be as large as 15–20 °C.

At first look at the measured temperature data, one might think that there are strong differences in heat flow in the Netherlands,

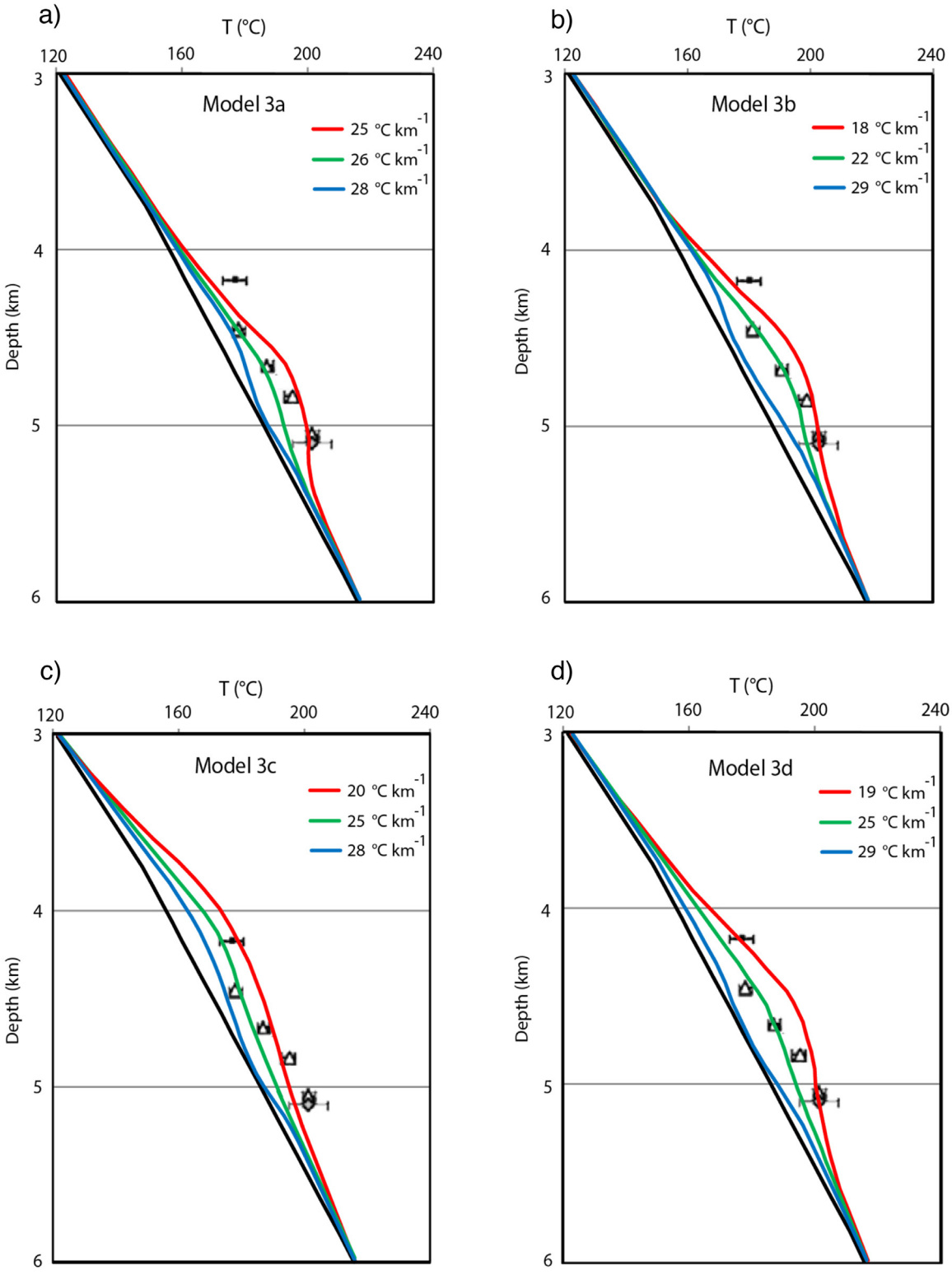

Fig. 13. Modelled temperature-depth profiles along three axes: upwelling (red curve), mixing zone (green curve) and downwelling (blue curve) for model 3 with a non-elevated gradient. Measured data from LTG-01 has been included for comparison. Black curve represents measured geothermal gradient. See Fig. 4 for explanation of symbols. (For interpretation of the references to colour in this figure legend, the reader is referred to the web version of this article.)

but models with a non-elevated temperature gradient show that this is not necessarily true (Figs. 12 and 13). Indeed, models 1 and 2, which consider a homogeneous permeability structure, overestimate the temperature within the Luttelgeest platform and result in elevated geothermal gradients both above and below the carbonate platform (Fig. 9). Even when the boundary conditions are changed and a lower geothermal gradient is applied (Fig. 10), the modelled gradients either overestimate the temperature (red curve) or the shape of the gradient through the platform is not a good fit (green curve). Model 3, which incorporates the heterogeneous nature of permeability in the inner platform and margin, provides a better fit (i.e. green curve in Fig. 13b). In fact, model 3 in Fig. 13 shows that at

large, the thermal gradient is not elevated at Luttelgeest, but rather it is locally elevated within the carbonate platform due to thermal convection.

7. Inferences for geothermal applications

The recent development of Enhanced geothermal systems (EGS) has enabled the utilization of medium-enthalpy reservoirs located in deep sedimentary basins (Limberger et al., 2014). Whereas most EGS projects worldwide have been exploiting granitic or sandstone reservoirs, the focus in the Netherlands is on deep carbonate formations. Deep carbonate platforms can be ideal locations for both thermal water use for direct heating and for electricity generation, by means of doublet systems consisting of an injection and production well (Goldscheider et al., 2010). However, geothermal installations in these reservoirs are characterized by high exploration risk if zones of increased permeability are missed. Detailed geological, geophysical and hydrogeological research is vital for reservoir assessment (Cloetingh et al., 2010; Goldscheider et al., 2010).

As the Netherlands is situated in a low to medium enthalpy environment, so far geothermal projects have exploited shallow formations (2–3 km) for direct heating purposes. To date no electricity has been generated from geothermal resources. For conversion to electricity, subsurface temperature and fluid flow conditions are critical parameters, as they control the thermal power and efficiency of electricity generation (DiPippo, 2007). As detailed in Section 3.1, the surface temperature in the Netherlands has an annual average of 10 °C and a geothermal gradient between 25 and 40 °C km^{-1}, with an average of 31 °C km^{-1}. This means that a minimum of 4–5 km must be drilled in order to reach sufficiently high temperatures for electricity production. At greater depths, porosity and permeability tend to decrease, and transmissivity becomes a challenge. In addition to increased risk of the investment, this implies that the aquifer may need hydraulic simulation before the well can be used, which adds to the cost and complexity of the investment.

If permeability is defined by a natural fracture network, as inferred for the Luttelgeest carbonate platform, hydraulic fracturing can be used to increase the connectivity between fractures within the fractured reservoir itself, as well as the connectivity of the fractured reservoir with injection and production wells. Injection of fluids at high pressure reduces the effective normal stress and may result in tensile fracking of the reservoir rock, thereby creating pathways for fluid flow. Pluymaekers et al. (2013) shows that fracking of a reference reservoir with a default permeability of 4 mD (4 10^{-15} m^2) and a thickness of 200 m can produce very high flow rates, suitable for production of electricity. The permeability values found at Luttelgeest and inferred by this study indicate that permeability can be one order of magnitude higher, illustrating that the Luttelgeest platform may have physical potential for the development of EGS. In future, the Luttelgeest platform can be used as an example reservoir to test a tensile hydraulic stimulation strategy. The levelised cost of energy (LCOE) can be calculated in future studies based on a techno-economic performance assessment (e.g. Van Wees et al., 2012).

8. Conclusion

The Dinantian carbonates encountered at the LTG-01 well in the Netherlands contains intervals of relatively high fracture permeability showing potential as a geothermal reservoir for electricity production. Temperature measurements indicate variations in subsurface temperature that could be indicative of convection. This is important, as convection creates areas where the temperature is anomalously high at shallow depths. For the purpose of geothermal energy exploration, it is of interest to know whether or not convection can occur in a particular reservoir, where convection cells are likely to develop and the temperature enhancements in the convective upwellings.

This study investigates the potential for thermal convection in the Luttelgeest carbonate platform We reproduce the thermal gradient at LTG-01 well using 3D numerical models of thermal convection. Numerical experiments test the effect of platform geometry and the permeability structure on the development of thermal convection and resulting temperature patterns.

Convective upwellings can create significant temperature enhancements relative to the conductive profile and in agreement with the observations in the Luttelgeest carbonate platform. This enhancement is critically dependent on the platform geometry and permeability structure. Both anisotropic permeability and the differentiation between margin and inner platform permeability play an important role in the distribution of heat due to convective fluid flow. Furthermore, numerical models show that the spacing of convective upwellings, and therefore spacing of thermal anomalies, can be predicted theoretically by knowing the platform thickness and permeability. The strong spatial variability of thermal anomalies in convective fractured aquifers at large depth can have a strong effect on exploration opportunity and risk of prospective areas. Numerical models can facilitate in exploration workflows to assess thermal variation and location of upwelling zones.

Acknowledgements

The research leading to these results has received funding from the European Community's Seventh Framework Programme under grant agreement No. 608553 (Project IMAGE). We thank Laurent Guillou-Frottier and an anonymous reviewer for their constructive comments, which have helped us to improve the manuscript.

References

Baillieux, P., Schill, E., Edel, J.B., Mauri, G., 2013. Localization of temperature anomalies in the Upper Rhine Graben: insights from geophysics and neotectonic activity. Int. Geol. Rev. 55 (14), 1744–1762.

Bjørlykke, K., Mo, A., Palm, E., 1988. Modelling of thermal convection in sedimentary basins and its relevance to diagenetic reactions. Mar. Petrol. Geol. 5, 338–351.

Bonté, D., Van Wees, J.-D., Verweij, J.M., 2012. Subsurface temperature of the onshore Netherlands: new temperature dataset and modelling. Geol. Mijnbouw-N. J. G. 91, 491–515.

Boro, H., Bertotti, G., Hardebol, N.J., 2013. Distributed fracturing affecting isolated carbonate platforms, the latemar platform natural laboratory (Dolomites, North Italy). Mar. Petrol. Geol. 40, 69–84.

Cherubini, Y., Cacace, M., Scheck-Wenderoth, M., Noack, V., 2014. Influence of major fault zones on 3-D coupled fluid heat transport for the Brandenburg region (NE German Basin). Geotherm. Energy Sci. 2, 1–20.

Cloetingh, S., van Wees, J.D., Ziegler, P.A., Lenkey, L., Beekman, F., Tesauro, M., Förster, A., Norden, B., Kaban, M., Hardebol, N., Bonté, D., Genter, A., Guillou-Frottier, L., Ter Voorde, M., Sokoutis, D., Willingshofer, E., Cornu, T., Worum, G., 2010. Lithosphere tectonics and thermos-mechanical properties: an integrated modelling approach for Enhanced Geothermal Systems exploration in Europe. Earth-Sci. Rev. 102, 159–206.

Collins, J.F., Kenter, J.A.M., Harris, P.M., Kuanysheva, G., Fischer, D.J., Steffen, K.L., 2006. Facies and reservoir-quality variations in the late Visean to Bashkirian outer platform, rim, and flank of the Tengiz buildup, Precaspian Basin, Kazakhstan, in: giant hydrocarbon reservoirs of the world: from rocks to reservoir characterization and modelling. SEPM Spec 88, 55–95.

De Jager, J., 2007. Geological development. In: Geology of the Netherlands. Royal Netherlands Academy of Arts and Sciences, Amsterdam, the Netherlands, pp. 5–26.

DiPippo, R., 2007. Ideal thermal efficiency for geothermal binary plants. Geothermics 36, 276–285.

Garibaldi, C., Guillou-Frottier, L., Lardeaux, J.M., Bouchot, V., 2010. Combination of numerical tools to link deep temperatures, geological structures and fluid flow in sedimentary basins: application to the thermal anomalies of the provence basin (South-East France). In: Proceedings World Geothermal Congress 2010, The International Geothermal Association, Bali, Indonesia.

Geluk, M.C., Dusar, M., de Vos, W., 2007. Pre-silesiam. In: Geology of the Netherlands. Royal Netherlands Academy of Arts and Sciences, Amsterdam, the Netherlands, pp. 27–42.
Goldscheider, N., Mádl-Szönyi, J., Eröss, A., Schill, E., 2010. Review: thermal water resources in carbonate rock aquifers. Hydrogeol. J. 18, 1303–1318.
Guillou-Frottier, L., Carré, C., Bourgine, B., Bouchot, V., Genter, A., 2013. Structure of hydrothermal convection in the Upper Rhine Graben as inferred from corrected temperature data and basin-scale numerical models. J. Volcanol. Geotherm. Res. 256, 29–49.
Holzbecher, E.O., 1998. Modeling Density-driven Flow in Porous Media: Principles, Numerics, and Software. Springer, Berlin, Germany, ISBN 3-540-63677-3.
Horton, C., Rogers, F., 1945. Convection currents in porous medium. J. Appl. Phys. 16 (6), 367–370.
Kühn, M., Dobert, F., Gessner, K., 2006. Numerical investigation of the effect of heterogeneous permeability distributions on free convection in the hydrothermal system at Mount Isa, Australia. Earth Planet. Sc. Lett. 244, 655–671.
Kenter, J.A.M., van Hoeflaken, F., Bahamonde, J., Bracco Gartner, G.L., Keim, L., Besems, R.E., 2002. Anatomy and lithofacies of an intact and seismic-scale Carboniferous carbonate platform (Asturias, NW Spain): analogues of hydrocarbon reservoirs in the Pricaspian Basin (Kazakhstan). SEPM Spec 74, 181–203.
Kombrink, H., Van Lochem, H., Van der Zwan, K.J., 2010. Seismic interpretation of Dinantian carbonate platforms in the Netherlands; implications for the palaeogeographical and structural development of the Northwest European Carboniferous Basin. J. Geol. Soc. 167, 99–108.
Kombrink, H., 2008. Tectonics and sedimentation in the northwest european carboniferous basin. In: The Carboniferous of the Netherlands and Surrounding Areas; a Basin Analysis, PhD Thesis. Universiteit Utrecht, pp. 21–46.
Lapwood, E., 1948. Convection in a porous medium. Proc. Camb. Phil. Soc. 44, 508–521.
Limberger, J., Calcagno, P., Manzella, A., Trumpy, E., Boxem, T., Pluymaekers, M.P.D., Van Wees, J.-D., 2014. Assessing the prospective resource base for enhanced geothermal systems in Europe. Geotherm. Energy Sci. 2, 1–15.
Lord Rayleigh, O.M.F.R.S., 1916. On convection currents in a horizontal layer of fluid, when the higher temperature is on the underside. Philos. Mag. Ser. 6 (32), 529–546.
Murphy, H.D., 1979. Convective Instabilities in Vertical Fractures and Faults. J. Geophys. Res. 1 (B11), 6121–6130.
Nield, D.A., Bejan, A., 2013. Convection in Porous Media. Springer, Berlin, Germany, ISBN 978-1-4514-5540-0.
Pasquale, V., Chiozzi, P., Verdoya, M., 2013. Evidence for thermal convection in the deep carbonate aquifer of the eastern sector of the Po Plain, Italy. Tectonophysics 594, 1–12.
Pluymaekers, M.P.D., Van Wees, J.D., Hoedeman, G.C., Fokker, P.A., 2013. Different Stimulation Strategies to Enhance the Performance of Subsurface Heat Exchangers Based on Tensile Fractures, Presented at Sustainable Earth Sciences Conference (SES) , European Association of Geoscientists and Engineers (EAGE), Pau, France.
Rabinowicz, M., Boulegue, J., Genthon, P., 1998. Two- and three-dimensional modelling of hydrothermal convection in the sedimented Middle Valley segment, Juan de Fuca Ridge. J. Geophys. Res. 103, 24045–24065.
Schilling, O., Sheldon, H.A., Reid, L.B., Corbel, S., 2013. Hydrothermal models of the Perth metropolitan area, Western Australia: implications for geothermal energy. Hydrogeol. J. 21, 605–621.
Sheldon, H.A., Florio, B., Trefry, M.G., Reid, L.B., Ricard, L.P., Ameed, K., Ghori, R., 2012. The potential for convection and implications for geothermal energy in the Perth Basin, Western Australia. Hydrogeol. J. 20, 1251–1268.
Tournier, C., Genthon, P., Rabinowicz, M., 2000. The onset of natural convection in vertical fault planes: consequences for the thermal regime in crystalline basements and for heat recovery experiments. Geophys. J. Int. 140, 500–508.
Van Hulten, F.F.N., Poty, E., 2008. Geological factors controlling Early Carboniferous carbonate platform development in the Netherlands. Geol. J. 43, 175–196.
Van Hulten, F.F.N., 2012. Devono-carboniferous carbonate platform systems of the Netherlands. Geol. Belg. 15, 284–296.
Van Oversteeg, K., Lipsey, L.C., Pluymaekers, M., van Wees, J.-D., Fokker, P.A., Spiers, C.J., 2014. Fracture Permeability Assessment in Deeply Buried Carbonates and Implications for Enhanced Geothermal Systems: Inferences from a Detailed Well Study at Luttelgeest-01, The Netherlands , Proceedings Thirty-Eighth Workshop on Geothermal Reservoir Engineering, Stanford University, Stanford, California.
Van Wees, J.D., Beekman, F., 2000. Lithosphere rheology during intraplate basin extension and inversion, inferences from automated modeling of four basins in western Europe. Tectonophysics 320, 219–242.
Van Wees, J.D., Kronimus, A., van Putten, M., Pluymakers, M.P.D., Mijnlief, H., van Hoof, P., Obdam, A., Kramers, L., 2012. Geothermal aquifer performance assessment for direct heat production—methodology and application to Rotliegend aquifers. Neth. J. Geosci. 91 (4), 651–665.
Weatherill, D., Simmons, C.T., Voss, C.I., Robinson, N.I., 2004. Testing density-dependent groundwater models: two-dimensional steady state unstable convection in infinite, finite and inclined porous layers. Adv. Water Resour. 27, 547–562.
Ziegler, P.A., van Wees, J.D., Cloetingh, S., 1998. Mechanical controls on collision-related compressional intraplate deformation. Tectonophysics 300, 103–129.